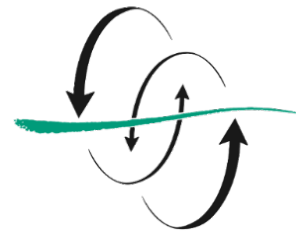


FACULTAD
DE CIENCIAS
DEL MAR



Western Boundary of the North Atlantic Subtropical Gyre: Decadal Change

Daniel Santana Toscano

Curso 2019/2020

Tutor: Dr. Alonso Hernández Guerra

Cotutora: Dra. María Dolores Pérez Hernández



Western Boundary of the North Atlantic Subtropical Gyre:
Decadal Change

por

Daniel Santana Toscano

Presentado en cumplimiento de los requisitos para:

MÁSTER EN OCEANOGRAFÍA

en

UNIVERSIDAD DE LAS PALMAS DE GRAN CANARIA

Firma del Autor.....

FACULTAD DE CIENCIAS DEL MAR

UNIVERSIDAD DE LAS PALMAS DE GRAN CANARIA

Firma del Tutor.....

INSTITUTO DE OCEANOGRAFÍA Y CAMBIO GLOBAL

DEPARTAMENTO DE FÍSICA

FACULTAD DE CIENCIAS DEL MAR

UNIVERSIDAD DE LAS PALMAS DE GRAN CANARIA

Firma de la Cotutora.....

INSTITUTO DE OCEANOGRAFÍA Y CAMBIO GLOBAL

DEPARTAMENTO DE FÍSICA

FACULTAD DE CIENCIAS DEL MAR

UNIVERSIDAD DE LAS PALMAS DE GRAN CANARIA

En Las Palmas de Gran Canaria a 17 de julio de 2020

Table of Contents

Abstract.....	1
1. Introduction	1
2. Data and Vertical Sections	2
2.1. Data.....	2
2.2. Hydrographic Sections.....	4
3. ADCP Velocities and Initial Transports.....	8
4. Inverse Box Model	9
5. Adjusted Meridional Transports.....	12
5.1. Heat and Freshwater Transports	15
6. Discussion.....	16
References	18

Abstract

The A20 is a meridional hydrographic section located at 52°W on the western North Atlantic Subtropical Gyre that encloses the main paths of the Atlantic Meridional Overturning Circulation (AMOC). Using data from two A20 hydrographic cruises carried out in 2003 and 2012 together with LADCP data and the velocities from an inverse box model, the circulation of the western North Atlantic Subtropical Gyre is estimated. The main poleward path of the AMOC is the Gulf Stream (GS) which carries 129.0 ± 10.5 Sv in 2003 and 110.4 ± 12.2 Sv in 2012. Due to the seasonality, the GS position is shifted southward in 2012 - relative to that of 2003 - as the cruise took place in Spring. In opposite direction, the Deep Western Boundary Current (DWBC) crosses the section twice, first at 39.3-43.2°N (-34.9 ± 7.5 Sv in 2003 and -25.3 ± 9.4 Sv in 2012) and then at 7.0-11.7°N (42.0 ± 8.0 Sv in 2003 and 48.0 ± 8.1 Sv in 2012). Two zonal currents contribute with westward transports, the North Equatorial Current at ca. 18°N (-5.2 ± 3.8 Sv in 2003 and -4.7 ± 3.1 Sv in 2012) and the North Brazil Current on the southern edge of the section (-22.8 ± 1.63 Sv and -32.0 ± 1.80 Sv for 2003 and 2012, respectively).

1. Introduction

From 1990 to 2002 the World Ocean Circulation Experiment (WOCE, <https://www.nodc.noaa.gov/woce/>) collected and analyzed hydrographic data across the globe. This experiment set the basis for the actual Global Ocean Ship-based Hydrographic Investigations Program (GO-SHIP). Both WOCE and GO-SHIP international programs organized the ship-based hydrographic surveys globally and established standard sections that allowed interannual comparisons. In addition, by creating an open-access database (<https://www.go-ship.org/About.html>), they rejoin the effort of individual countries and gave visibility to single surveys.

The western basin of the North Atlantic Subtropical Gyre is the main source of the warm poleward waters that feed the upper limb of the Atlantic Meridional Overturning Circulation (AMOC). The main northward path for these waters towards higher latitudes flows along the north American slope and it is called the Gulf Stream (GS). Though part of the GS flow recirculates on the eastern Subtropical Gyre southward (Pérez-Hernández et al., 2013; Pérez-Hernández et al., 2015; Vélez-Belchí et al., 2017), most of it flows northward to high latitudes where it interacts with the cool atmosphere and becomes colder, denser and, therefore, sinks into the deep layers of the ocean (Pérez-Hernández et al., 2019; Våge et al., 2013). Underneath the GS, also expanding over the western Subtropical Gyre, the Deep Western Boundary Current (DWBC) forms the lower limb of

the AMOC and is the main southward flow carrying dense cold water formed at high latitudes (Bower et al., 2019).

The meridional A20 section expands along 52°W over the western North Atlantic Subtropical Gyre where the main currents of the AMOC lay. It was firstly sampled in 1997, and, later, in autumn of 2003 and spring of 2012, two meridional hydrographic sections reoccupied it. The main objectives of these cruises were to portray and quantify a snapshot of the water mass distribution and circulation pattern of the western boundary of the North Atlantic Subtropical Gyre. Climate variability was also an objective of these cruises as this section was firstly occupied in 1997 and studied later in Joyce et al. (1999) and Hall et al. (2004). Data acquisition and treatment have developed greatly year by year. Thus, the oceanic and climatic variations can be studied with better resolution in comparison to previous works, where slight changes in patterns/distributions could be lost in data uncertainty. Thanks to GO-SHIP, the A20 section can also provide with spatial information by contrasting it with other sections nearby. This allows a deeper understanding of the up/downstream evolution of the current. For the A20, it is worth comparing transports and water mass estimations with the A22 meridional section existing at nominal 66°W described in Joyce et al. (2001) and Casanova-Masjoan et al. (2018).

In this work, the decadal changes of these transports - and other weaker flows - will be studied as well as the heat and the freshwater flows. The study is organized as follows: Section 2 presents the hydrographic and Lowered Acoustic Doppler Current Profiler (LADCP) data acquired on 2003 and 2012 cruises as well as the water masses present on each year; Section 3 introduces the initial geostrophic velocities estimates and the unbalanced transports computed from them; Section 4 explains the usage of the inverse box model for the estimation of the absolute velocity field; Section 5 presents the inverse box model output and the adjusted geostrophic mass and silica transports; Section 6 presents the heat and freshwater fluxes for both years; and finally in Section 7, we sum up with the discussion over the main results and changes between 2003 and 2012.

2. Data and Vertical Sections

2.1. Data

Hydrographic data of two meridional cruises were collected along the A20 section at nominally 52°W in the North Atlantic. The cruises took part in autumn 2003 (September 22 to October 20) and spring 2012 (April 19 to May 15) as part of the international GO-SHIP program (Talley et al., 2016). The 2003 cruise started sampling at the Grand Banks of Newfoundland and ended in French Guiana, whereas the 2012 cruise was carried out

inversely, from French Guiana to the Grand Banks (Fig. 1). The rosette was equipped with a SBE9plus Conductivity-Temperature-Depth sensor (CTD) and with LADCP. LADCP/CTD/rosette data were obtained for the entire water column at every station for both cruises, only the 4 last stations of the 2003 cruise lacked LADCP data (stations 85-88). For the 2003 cruise, an upward looking 300 kHz LADCP and downward looking 150 kHz LADCP were set, while for the 2012 cruise, there was only a downward looking 150 kHz LADCP. Both cruise reports and details of the measurements can be found at the CLIVAR and Carbon Hydrographic Data Office (CCHDO) webpage (<https://cchdo.ucsd.edu/>). Wind data from the National Centers for Environmental Prediction (NCEP-DOE) Reanalysis II project from the National Oceanic and Atmospheric Administration (NOAA) are used to estimate the Ekman transports (<https://psl.noaa.gov/data/gridded/data.ncep.reanalysis2.html>; Kanamitsu et al., 2002).

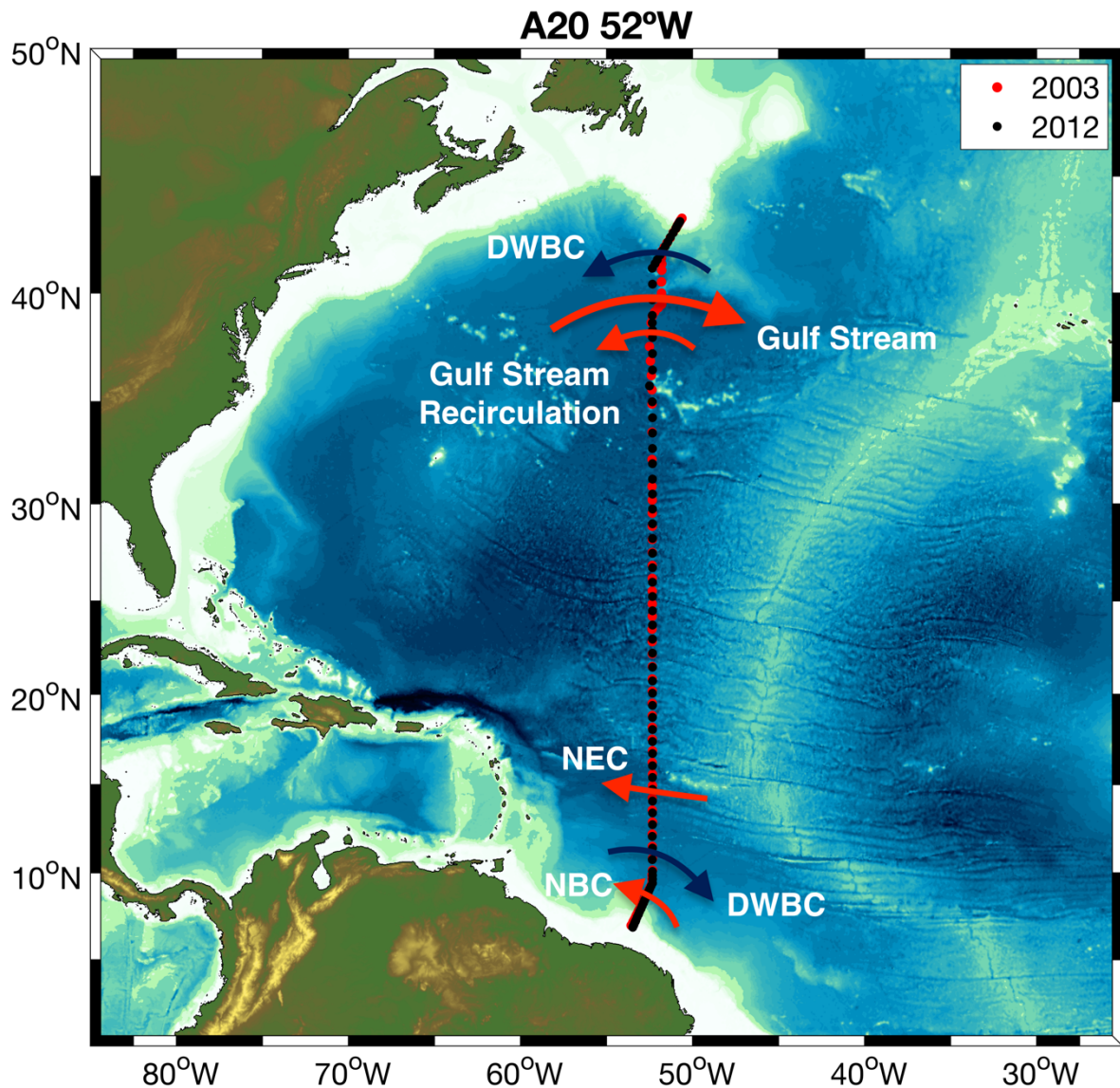


Figure 1. Location of the hydrographic stations surveyed for the A20 section in 2003 (red dots) and 2012 (black dots). Arrows designate major currents through the section. DWBC: Deep Western Boundary Current. NEC: North Equatorial Current. NBC: North Brazil Current.

2.2. Hydrographic Sections

Potential temperature-salinity (θ -S) diagrams (Fig. 2) and vertical sections of potential temperature (θ), salinity, neutral density, silica- and oxygen concentrations (Figs. 3–7) are used for water masses determination. As a consequence of seasonality, the 2003 surface waters reach values of potential temperature higher than 25°C and values of salinity higher than 37, whereas the 2012 surface waters are colder and fresher, reaching 25°C only regionally at the southern end and barely presenting salinities higher than 37 (Figs. 2-4).

A branch of the 2012's Amazonian Waters appears in Fig. 2B in light blue, the salinities within these waters extend as low as 26 (not shown in Figure 2B for the sake of comparison) over a narrow temperature range of 27-28°C. As this phenomenon only occurred in 2012, only one salinity patch of Amazonian Water can be seen in the first meters of Fig. 4 at 5-10°N latitudes. A similar phenomenon occurred also in 1997, as studied by Hernandez-Guerra & Joyce (2000).

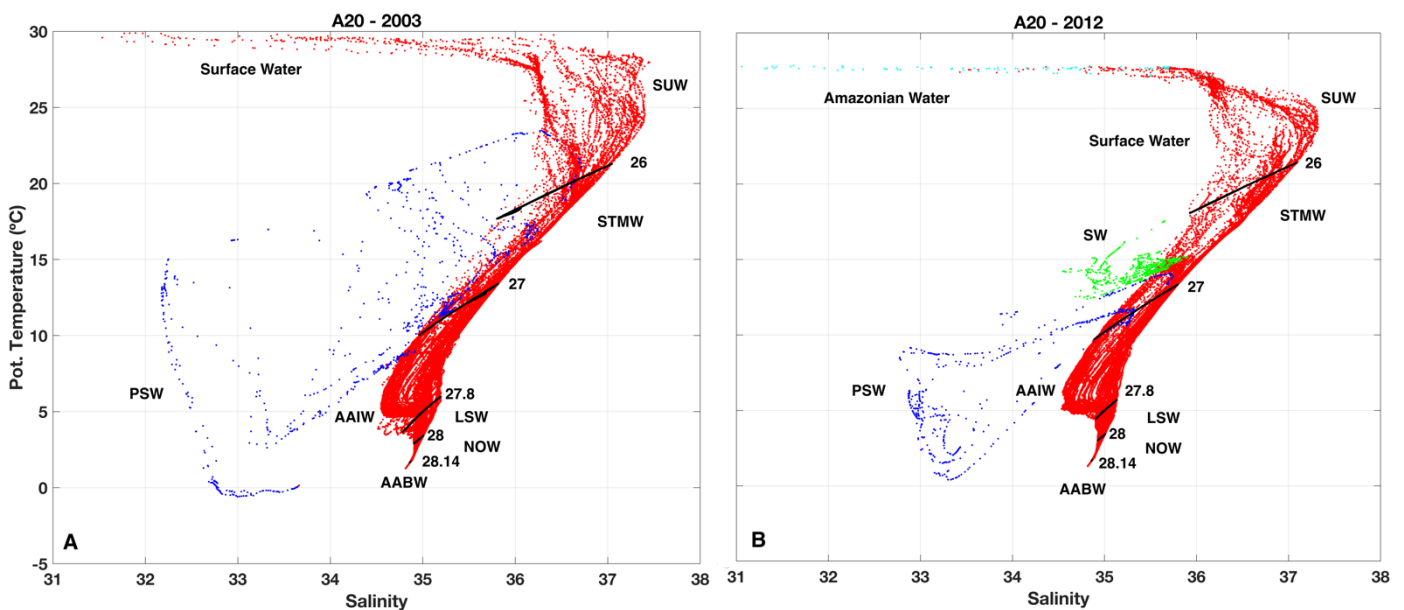


Figure 2. θ -S diagrams for 2003 (A) and 2012 (B). Black lines are the selected neutral density layers of 26, 27, 27.8, 28 and 28.14 kg m^{-3} . Red dots indicate the main body of the θ -S diagrams. Dark blue dots refer to Polar Surface Water (PSW), green dots to Slope Water (SW) and light blue dots to Amazonian Water.

Polar Surface Water (PSW) has been dragged by the Labrador Current from high latitudes. It originates in the Arctic Ocean as a combination of river runoff, ice melt and mixing with the lower layers (Little et al., 2019). It appears clearly as a dark blue patch in the first 250 m between 40-45°N latitudes (Fig. 4). In Fig. 2, PSW is the set of scattered dots between 0-20°C and salinities between 32-35 highlighted in dark blue.

Slope Waters (SW) can be found in the 2012's θ -S diagram (Fig. 2B) as a branch of salinities between 34.5-36 and θ between 10-15°C. This water mass also flows south with the Labrador current and occupies the surface-to-subsurface layers ($26.0 < \gamma^n < 27.0 \text{ kg m}^{-3}$) northernmost part of the section, being limited by the GS in Figure 5.

The GS signal is shown as steep ascending isopycnals between 35-40°N latitudes (Fig. 5) (Lillibridge et al., 1990). As a matter of fact, the GS shallows the isopycnals (Fig. 5) producing an eastward net transport. Just south of it, at nominally 35°N latitude, the isopycnals behavior is the opposite, implying the existence of a westward transport named the GS Recirculation (GSR; Fig. 5). Figure 5 shows that the GS isopycnal is found at slightly higher latitudes in 2012 than in 2003.

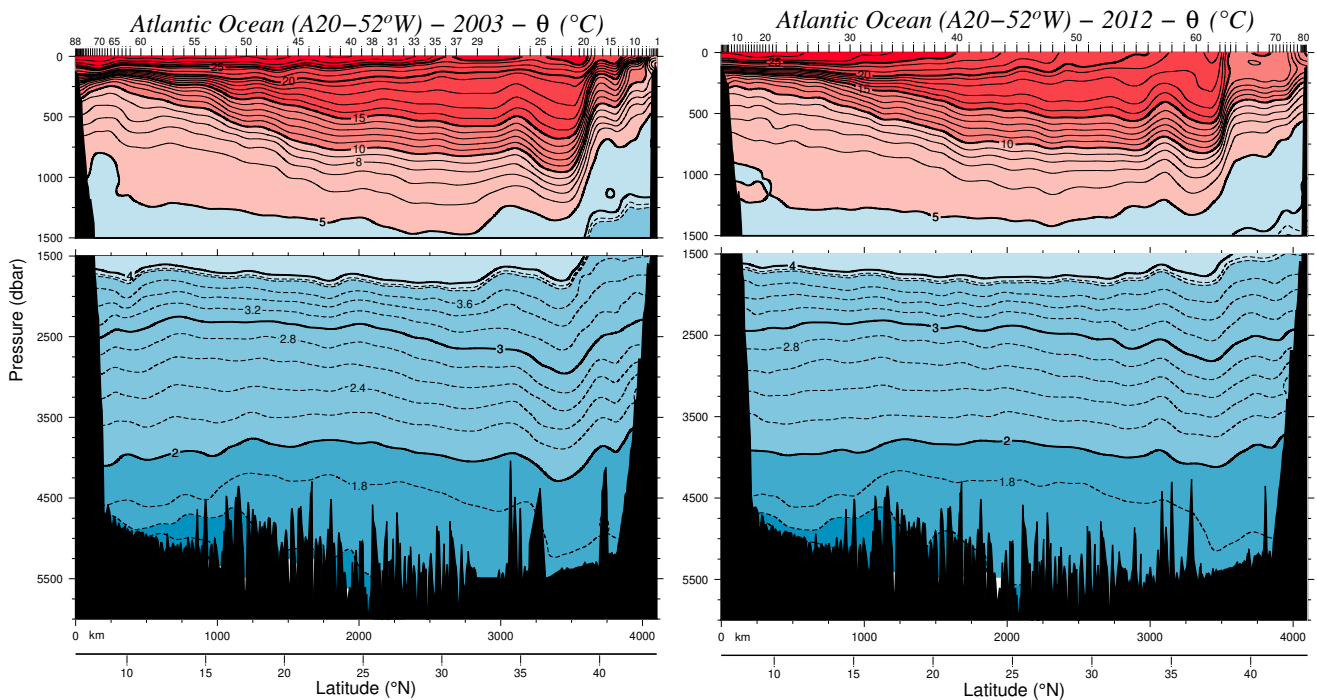


Figure 3. Potential temperature (°C) vertical sections for 2003 (left) and 2012 (right).

On both years, south of the GS and between the 16-18°C isotherms (Fig. 3), 36-36.5 isohalines and 250-500 m depth (Fig. 4) appears the subtropical mode water (STMW), which is formed by convection in late winter south of the GS (Joyce et al., 2013). It can also be seen in the θ -S diagram at salinities of 36-36.5 and θ of 16-18°C (Fig. 2).

As described in Metcalf (1976) and Casanova-Masjoan et al. (2018), the North Atlantic Subtropical UnderWater (SUW) appears as a maximum salinity (>36.5) water mass in the upper layers of the southern side of the section from latitudes 5-15° (Fig. 3). It is created as the result of the positive rate of evaporation/precipitation in the central tropical Atlantic.

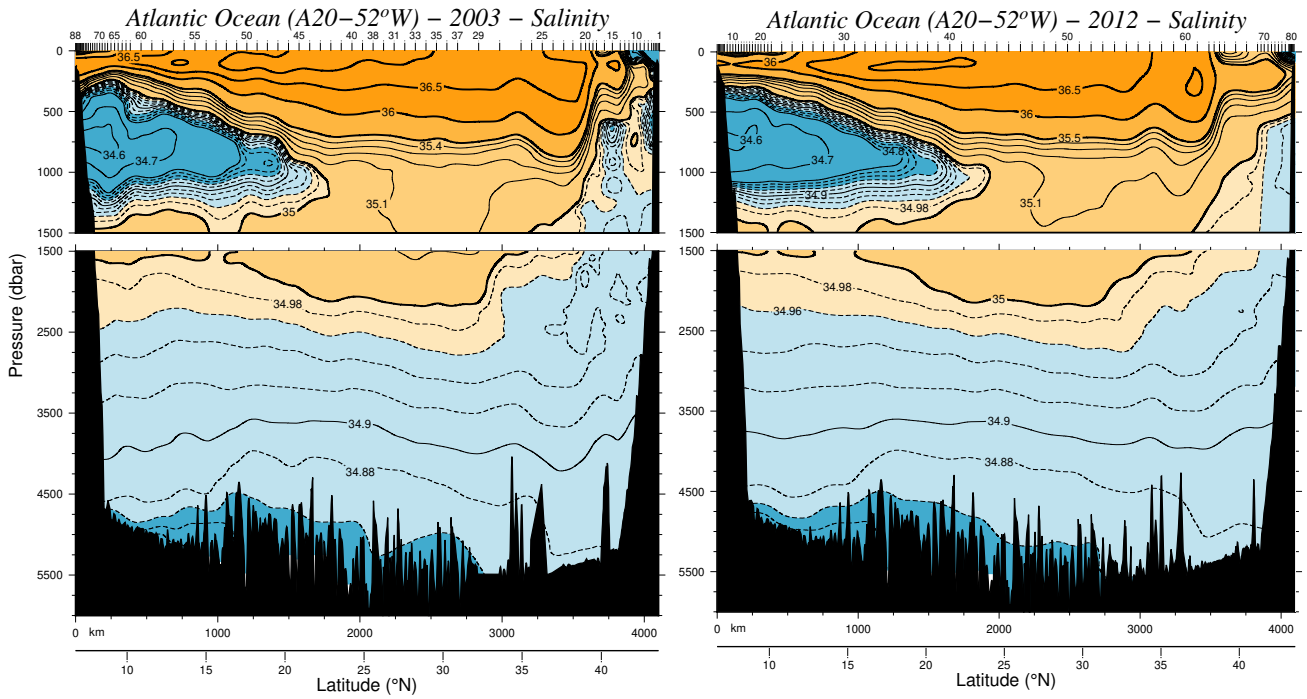


Figure 4. Salinity vertical sections for 2003 (left) and 2012 (right).

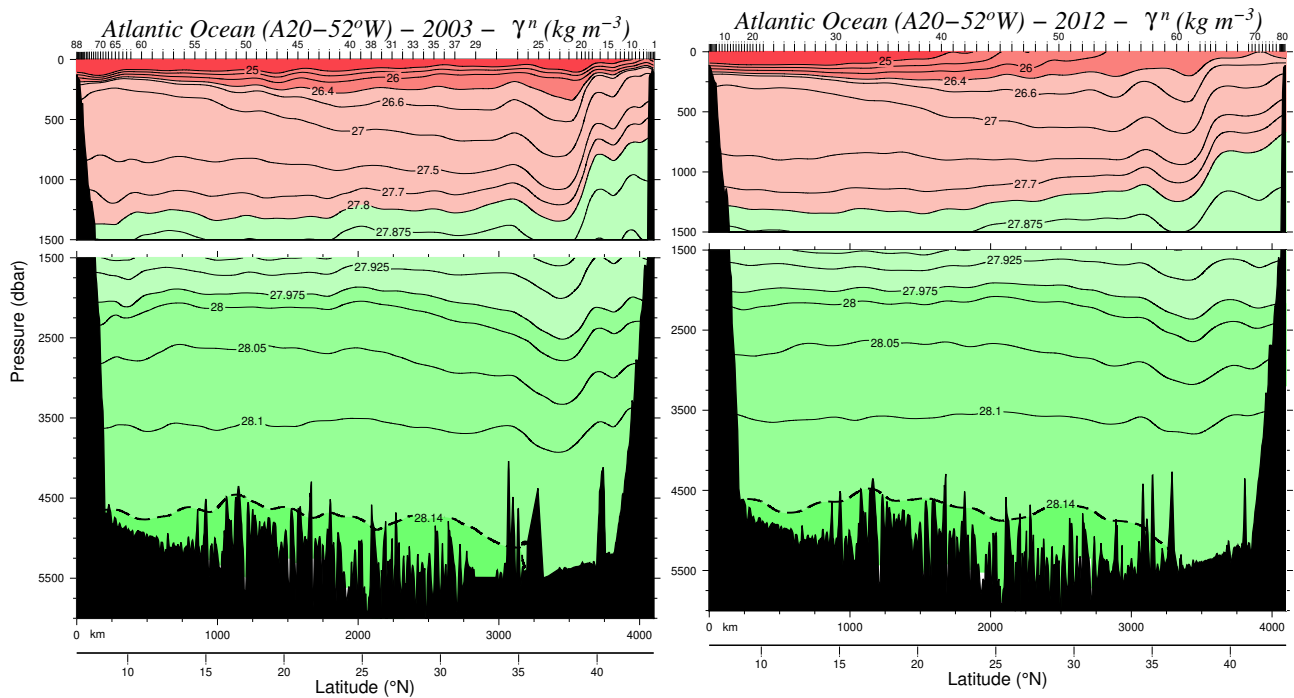


Figure 5. Neutral density (kg m^{-3}) vertical sections for 2003 (left) and 2012 (right). The dashed isopycnal indicates the reference level of no motion for the initial transports.

As occurred with PSW and SW, Labrador Sea Water (LSW) has also been dragged from the north by the Labrador Current. It arrives at approximately 40°N with temperatures of $3\text{-}5^\circ\text{C}$ (Fig. 3), salinities relatively low that stand out in Figure 4 (between $34.94\text{-}35$), neutral densities of $27.8\text{-}28 \text{ kg m}^{-3}$ (Fig. 5) and remarkably high oxygen concentrations exceeding the $200 \mu\text{mol kg}^{-1}$ (Fig. 7). It can also be seen in the $\theta\text{-S}$ diagram

at salinities of ~ 35 and θ of $\sim 5^\circ\text{C}$ (Fig. 2). The LSW is carried on southward through the whole section deepening on the GS latitude until almost 2500 m depth.

Antarctic Intermediate Water (AAIW) is depicted by the low salinity (Fig. 4), high silica (Fig. 6) and low oxygen water lobe found at 250-1250 m depth and about $5\text{-}10^\circ\text{N}$ latitude. It can also be found in the θ -S diagram at the $35\text{-}5^\circ\text{C}$ pair of data.

Viewing the section from the north to the south, the elevation of the deep isopycnals (Fig. 5) depict the presence of the DWBC from 750 m to the bottom of the ocean, crossing westwards the section at $>40^\circ\text{N}$ latitude. A similar deep and steep isopycnal change can be found looking from south to north at $<10^\circ\text{N}$ latitude, but this time it crosses eastwards, continuing its path to the Equator. In terms of oxygen concentration, its trademark is the $>260 \mu\text{mol kg}^{-1}$ values from 750 m depth to the bottom of the ocean (Fig. 7).

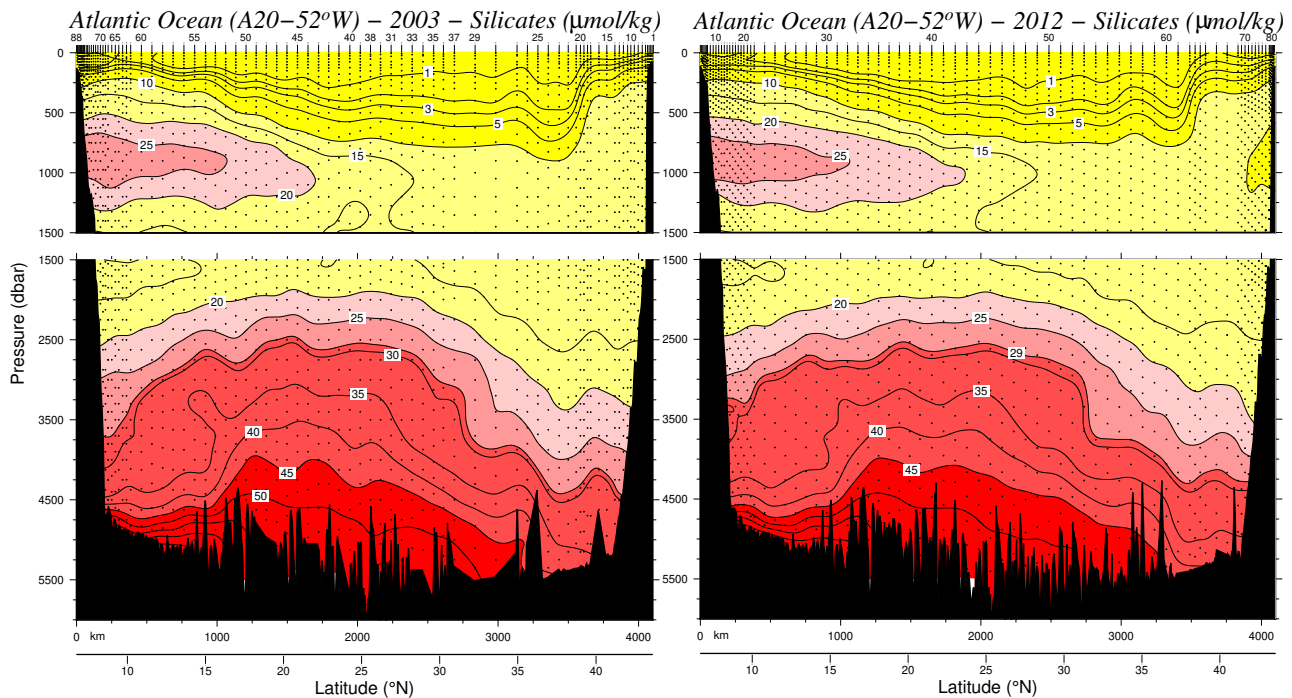


Figure 6. Silicates concentration ($\mu\text{mol kg}^{-1}$) vertical sections for 2003 (left) and 2012 (right).

Looking carefully into the 2012's oxygen section (Fig. 7), the presence of values over the $270 \mu\text{mol kg}^{-1}$ threshold may define at least two different water masses in the north: one at ~ 1000 m depth, which is the LSW, and one at 2000-4500 m depth, which is the Nordic Overflow Water (NOW). NOW is the name of the group of waters masses formed by Iceland-Scotland Overflow Water (ISOW) and Denmark Strait Overflow Water (DSOW) (Smethie, 1993). The deep ascending isopycnals (Fig. 5) and silica isolines (Fig. 6) north of French Guiana and at latitudes $>35^\circ\text{N}$ reveals the presence of Lower Deep Water (LDW). LDW is the result of the mixture between NOW and Antarctic Bottom Water (AABW) (Hall et al., 2004; Joyce et al., 1999). This water mass, along with the other northern water masses (LSW and NOW) conforms the so-called North Atlantic

Deep Water (NADW) that is the main water mass that is carried equatorward by the DWBC.

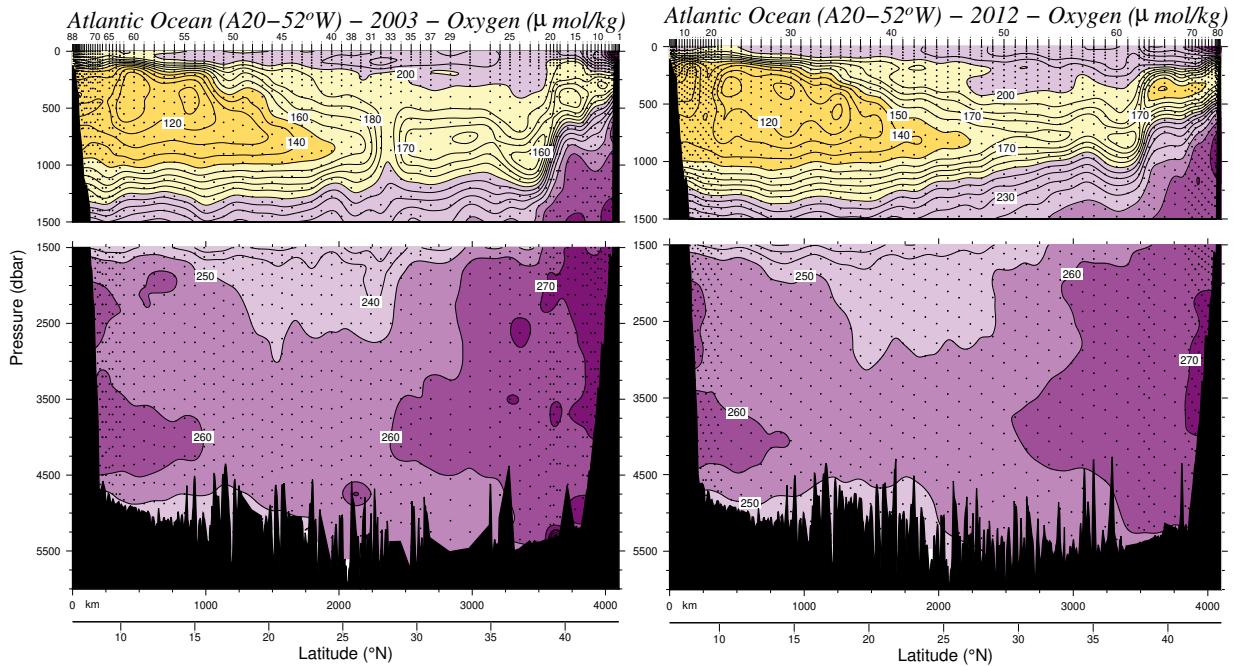


Figure 7. Oxygen concentration ($\mu\text{mol kg}^{-1}$) vertical sections for 2003 (left) and 2012 (right).

The deepest and densest water mass in the section is the AABW. This water mass is only observed south of 35°N and deeper than 4500 m depth. It is a low temperature- high silicate- water mass with θ under 1.6°C (Fig. 3) and silica concentrations over $50 \mu\text{mol kg}^{-1}$ (Fig. 6). The isoneutral line that defines the AABW is the 28.14 kg m^{-3} (Fig. 5, dashed line).

3. ADCP Velocities and Initial Transports

The initial geostrophic velocity is computed for each station pair using the thermal wind equation. In order to estimate the geostrophic velocity, a reference level of no motion has to be chosen. Following Casanova-Masjoan et al. (2018) and Joyce et al. (2001), the reference level is chosen between the LDW and the AABW, as they flow in opposite directions. The isoneutral line that defines this separation is $\gamma^n = 28.14 \text{ kg m}^{-3}$ (dashed line, Fig. 5). When the seafloor is shallower than that level, the deepest layer at that station pair is used as the level of no motion.

The comparison between CTD initial geostrophic velocity and LADCP velocity shear is generally bound to be noisy as the CTD initial geostrophic velocity averages the velocities by the distance between stations while the LADCP in situ measurements include all ageostrophic and geostrophic components measured in each station and later averaged in each station pair. Thus, only the best confluent profiles at certain depths (Fig.

8) have been chosen to select the velocities at the reference level (Comas-Rodríguez et al., 2010).

The 2003 and 2012 LADCP and initial geostrophic velocity profiles at the Gulf Stream (Fig. 8. A, C) are shown as an example of a very good agreement. This is a particle-rich zone of the ocean and thus the LADCP doppler effect works proficiently. In contrast, in the oligotrophic Mid-Atlantic zone (Fig. 8B), the agreement is rougher, although it can be made by using selected depths in 2003. For some station pairs, the LADCP is not useful as the differences with the initial geostrophic velocity were unbridgeable (Fig 8D). For the 2003 cruise, a total of 50 stations pairs are adjusted using LADCP measurements, whereas in 2012, only 31 stations pairs could be adjusted.

The initial unbalanced net mass transports for 2003 and 2012 cruises are 30.0 Sv and -178.9 Sv, respectively (Fig. 9A). For silica, the unbalanced net transports for 2003 and 2012 are -241.8 kmol/s and -4176.9 kmol/s, respectively (Fig. 9B).

The mass transport structure heavily differs from isoneutral layers $26-27.7 \text{ kg m}^{-3}$: in 2003 (blue line) the intermediate transport shows a maximum, whereas in 2012 (black line) shows a minimum in shallower depths (Fig. 9). The rest of the water column has the same distribution with different magnitudes. The upper layers presented an almost zero silica transport because of the low silica concentration in this region (Fig. 6). As a counterpart, the intermediate to bottom silica transports are highly correlated with the mass transport as they had high silica concentrations from $\gamma^n = 27.975 \text{ kg m}^{-3}$ (approximately 2000 m) to the seafloor (Figs. 5, 6). The AAIW at $27.0 < \gamma^n < 27.7 \text{ kg m}^{-3}$ (500-1000 m depth, Fig. 5) created the slightly positive silica transport between these layers (Fig. 9B), as this water mass had a medium-to-high silica concentration (Fig. 6).

The surface adjusted geostrophic transports underwent through another step. The net Ekman transport has been included in the first layer of the transect. These values are $-0.07 \pm 0.16 \text{ Sv}$ for 2003 and of $-0.33 \pm 0.15 \text{ Sv}$ for 2012 (negative values implying westward transport). For a better comparison with previous studies, these values have been estimated at the same time interval of each cruise (Hall et al., 2004; Joyce et al., 2001).

4. Inverse Box Model

After the thermal wind equation is used to estimate the initial geostrophic transport and geostrophic velocities have been adjusted with in situ measurements, the inverse box model come to hand as an efficient tool to further adjust the velocities in the reference level. We have followed the studies of Casanova-Masjoan et al. (2018), Hall et al. (2004) and Joyce et al. (2001) and used the same 17 neutral surface layers. The model uses a set of constraints, and their respective uncertainties, which must be introduced as the model's

input. The most important constraint is the mass conservation: the mass of an enclosed water volume must be preserved; thus, mass cannot be neither created nor destroyed inside the enclosed volume (Casanova-Masjoan et al., 2018; Wunsch, 1978, 1996).

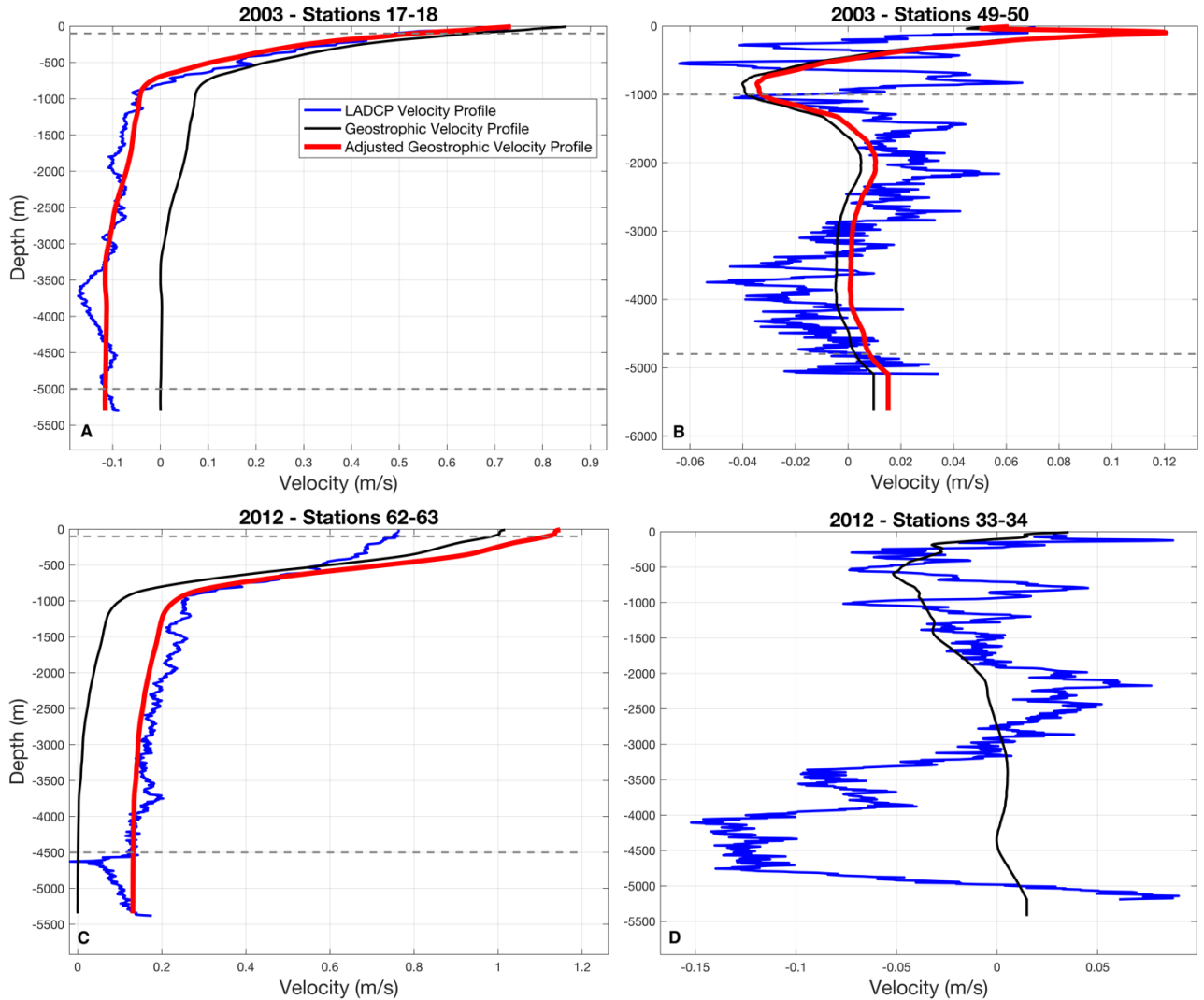


Figure 8. Three examples of LADCP velocity profiles used to reference the geostrophic velocity (A-C) and one that was not used (D). LADCP perpendicular to each station pair (blue), geostrophic velocity referred to the initial level of no motion (black) and LADCP adjusted geostrophic velocity (red). (A), (C) 2003 and 2012's Gulf Stream, respectively; (B), (D) 2003 and 2012's Mid-Atlantic, respectively.

The mass and silica constraints are homologous when introduced in the inverse model. Constraints 1 and 19 are the total mass and total silica conservation, respectively. Constraints 2-18 and 20-36 are the mass and silica conservation per each neutral density layer (shallowest to deepest), respectively. The Ekman transport has been added only in the total mass conservation and in the shallowest layer of the mass conservation per layers taking into account the outcropping (constraint 2).

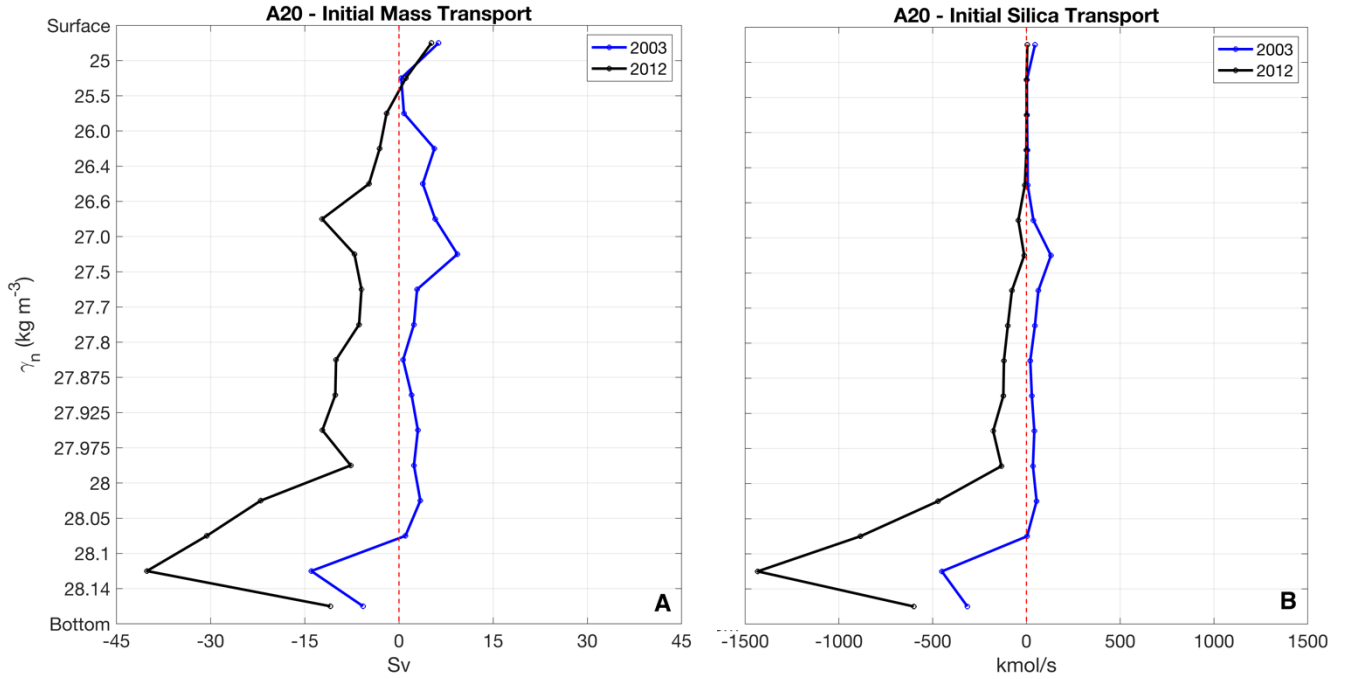


Figure 9. Initial meridionally integrated mass (A) and silica (B) transports (in Sv and kmol/s , respectively). Blue lines correspond to 2003 transports and black lines correspond to 2012 transports.

As shown in Casanova-Masjoan et al. (2018), the matrix equation can be formulated as follows:

$$Ab+n=Y$$

where A is an $M \times N$ matrix being M the number of constraints and N , the number of unknowns, b is a $N \times 1$ column vector with the unknown geostrophic reference velocities for each of the N^{th} station pairs, n is a column vector of length M with the noise of each constraint, and Y is a vector representing the initially unbalanced mass transport.

This inverse problem has more unknowns than equations and, therefore, we use the Gauss–Markov method to solve it. The method provides a solution for the initial estimates with error variances as minimum as possible (Wunsch, 1996). Thus, two sets of a priori variances are required: one for the constraints and one for the velocities. Following Joyce et al. (2001), we have chosen the velocity variances as $(0.05 \text{ m s}^{-1})^2$ for the LADCP-referred velocities and $(0.1 \text{ m s}^{-1})^2$ for the non-LADCP-referred velocities. The mass variances are $(0.5 \text{ Sv})^2$ for the total mass conservation, $(2 \text{ Sv})^2$ for the 4 shallowest layers and $(1 \text{ Sv})^2$ for the next layers. In terms of silica concentration, the variances are $(5 \text{ kmol s}^{-1})^2$ for the total silica conservation, $(20 \text{ kmol s}^{-1})^2$ for the first four layers and $(10 \text{ kmol s}^{-1})^2$ for the rest.

Thus, the inverse model is applied to the water volume enclosed by the American coastline to the south and north and the A20 section to the east. There is not a significant

flow through the Panama Canal (Joyce et al., 2001), so the volume is considered to be fully enclosed in the west, too.

Table 1. Neutral density layers γ^n (kg m^{-3}), layer numbers, level of no-motion (bold) and water masses (Casanova-Masjoan et al., 2018; Hall et al., 2004; Joyce et al., 2001).

γ^n	Layer Number	Water Mass
20-25	1	Surface Layer
25-25.5	2	Upper Thermocline
25.5-26	3	SUW
26-26.4	4	Upper Thermocline
26.4-26.6	5	STMW
26.6-27	6	Lower Thermocline
27-27.5	7	AAIW
27.5-27.7	8	AAIW
27.7-27.8	9	AAIW
27.8-27.875	10	ULSW
27.875-27.925	11	LSW
27.925-27.975	12	CLSW
27.975-28	13	ISOW
28-28.05	14	ISOW
28.05-28.1	15	DSOW
28.1- 28.14	16	LDW
28.14 -29	17	AABW

5. Adjusted Meridional Transports

As in Fig. 9, the meridionally integrated final mass and silica transports for 2003 and 2012 are estimated after the inverse model (Fig. 10). The error bars only represent errors due to the inverse model. Net mass transports for 2003 and 2012 are 0.20 ± 2.0 Sv and -1.7 ± 2.2 Sv, respectively (Fig. 10A). Net silica transports for 2003 and 2012 are 34.0 ± 27.0 kmol/s and 3.32 ± 25.7 kmol/s, respectively (Fig. 10B). Note the great magnitude reduction in both vertical distributions when compared to the initial transports (Fig. 9). As the mass

transport for both years is not significantly different from zero, we have achieved mass balance across the sections, hence we proceed to estimate the transport of each current.

In this case, the mass transport structure follows almost the same distribution for both years differing slightly in magnitude (note the colliding error bars at several depths). For the silica transport (Fig. 10B), differences can only be noted at the first layer - maximum negative silica transport for 2003 and slightly positive for 2012 - and between the isoneutral layers $27.7-27.8 \text{ kg m}^{-3}$ - 2003's transport is not significantly different from zero while the 2012's transport is significantly negative - because of the low silica concentration in this region (Fig. 6). The AAIW at $27.0 < \gamma^n < 27.7 \text{ kg m}^{-3}$ (500-1000 m depth, Fig. 5) created the slightly positive silica transport between these layers (Fig. 9B), as this water mass had a medium-to-high silica concentration (Fig. 6).

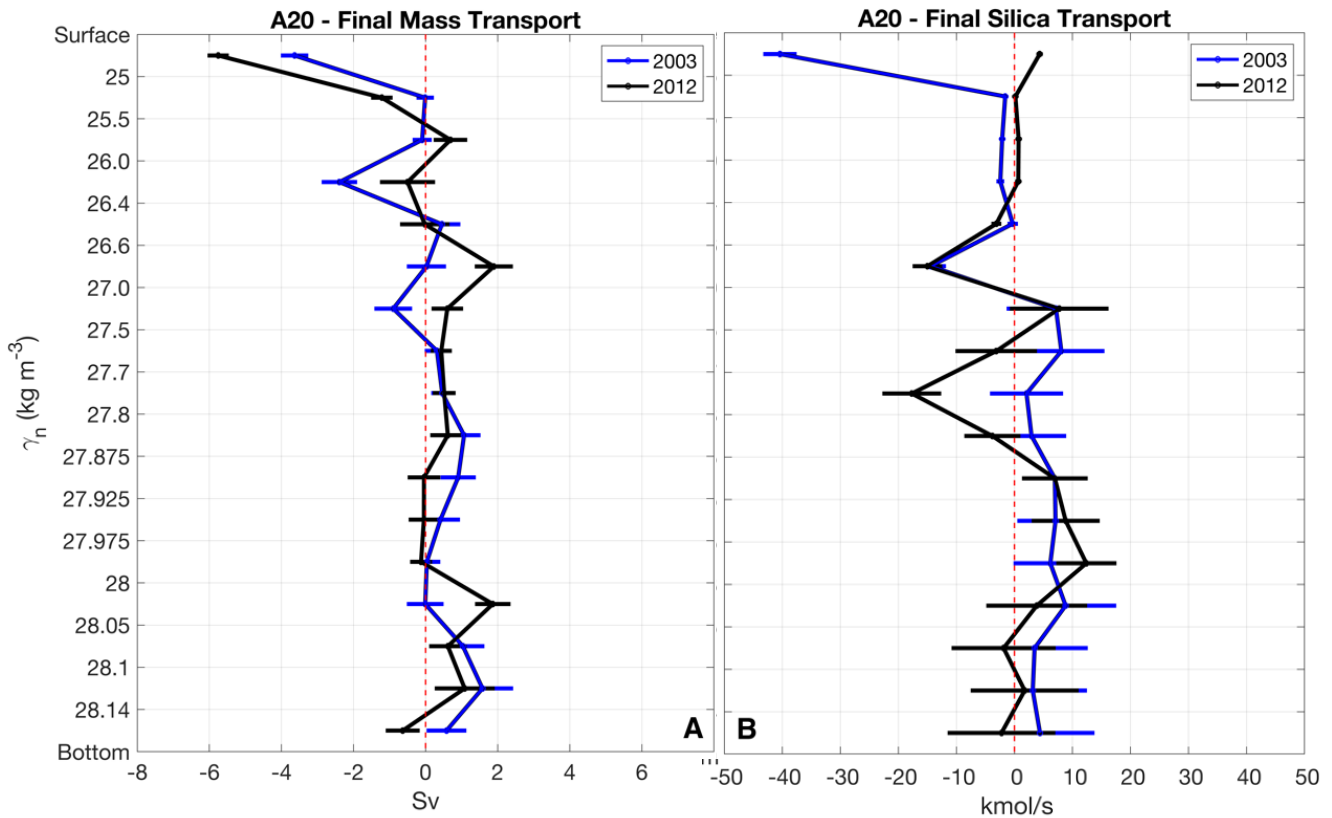


Figure 10. Final meridionally integrated mass (A) and silica (B) transports (in Sv and kmol/s , respectively). Blue lines correspond to 2003 transports and black lines correspond to 2012 transports.

Four major meridional transport systems flow through the A20 section (Fig. 1). From north to south, the current systems are: Labrador Current (LC), DWBC, GS and its recirculation (GSR), North Equatorial Current (NEC) and North Brazil Current (NBC); note that the DWBC flows two times through 52°W , at the northern side ($39.3-43.2^\circ\text{N}$) and southern side ($7.0-11.7^\circ\text{N}$) latitudes.

The DWBC carries westward the different components of LSW and NOW (layers 10 to 16). The transport of the northern DWBC is estimated as the sum of the transports existing at the deep layers between 39.3-43.2°N (Fig. 11D). This gives a transport of -34.9 ± 7.5 Sv for 2003 and -25.3 ± 9.4 Sv for 2012 (Table 2). The result for 2012 is not significantly different from those estimated by Macdonald (1998): -14 ± 5 Sv (36°N); and by Ganachaud (2003): -16 ± 2 Sv (48°N) when the uncertainties are taken into account. On top of the northern DWBC (layers 1 to 9) we found the Labrador Current (LC), which flows westward with the DWBC from the Labrador Sea and has been historically differentiated from it as it carries Polar Surface Water (Fig. 2, dark blue colors). The LC transport for 2003 is -0.80 ± 1.4 Sv and -0.15 ± 0.18 Sv for 2012 (Figs. 11B, C). These values are lower than the 5 Sv described in Han & Tang (1999) at Newfoundland using altimetry. The reason for this difference is that both cruises started on the slope located south of the Grand Banks of Newfoundland while the shelf remain unsampled.

The 2003 GS and GSR can be found between 37.3-39.3°N and 35.2-37.3°N respectively, while in 2012, GS and GSR shifted slightly to the south and are observed at 36.9-38.8°N and 34.6-36.9°N, respectively (Fig. 11A). Both the GS and the GSR have been estimated as the net vertical transport along the above-mentioned latitudes. The transport of the GS is 129.0 ± 10.5 Sv and 110.4 ± 12.2 Sv for 2003 and 2012, respectively. On the other hand, the recirculation transport is -88.2 ± 12.0 Sv and -89.8 ± 15.1 Sv for 2003 and 2012, respectively. The small differences in the GS system transport between the two years may be caused by seasonality, as demonstrated by Sato & Rossby (1995). In addition, the GS is on average more northerly in fall and more southerly in spring (Rayner et al., 2011; Tong Lee & Cornillon, 1995; Tracey & Watts, 1986), which agrees with our observations.

Next on the line appears the westward NEC (Fig. 1; Hormann et al., 2012). Superficial and intermediate layers have been used for the transport estimation as well as the latitude range of 9.0°N-23°N (Figs. 11B, C). The transports are -5.2 ± 3.8 Sv and -4.7 ± 3.1 Sv for 2003 and 2012, respectively. So, there is no significant alteration of the NEC between the two years.

The NBC flows through layers 1-9 towards the Caribbean basin (westwards) between 7.0-9.0°N latitudes with values of -22.8 ± 1.63 Sv and -32.0 ± 1.80 Sv for 2003 and 2012, respectively (Fig. 11B). Just deeper from the NBC (layers 10-16) and occupying almost the same latitudes, flows the southern tip of the DWBC. In this case, latitudes go as high as 11.7°N. The DWBC transports equatorward 42.0 ± 8.0 Sv for 2003, slightly higher than the value estimated in Hall et al. (2004) that was 32 Sv.

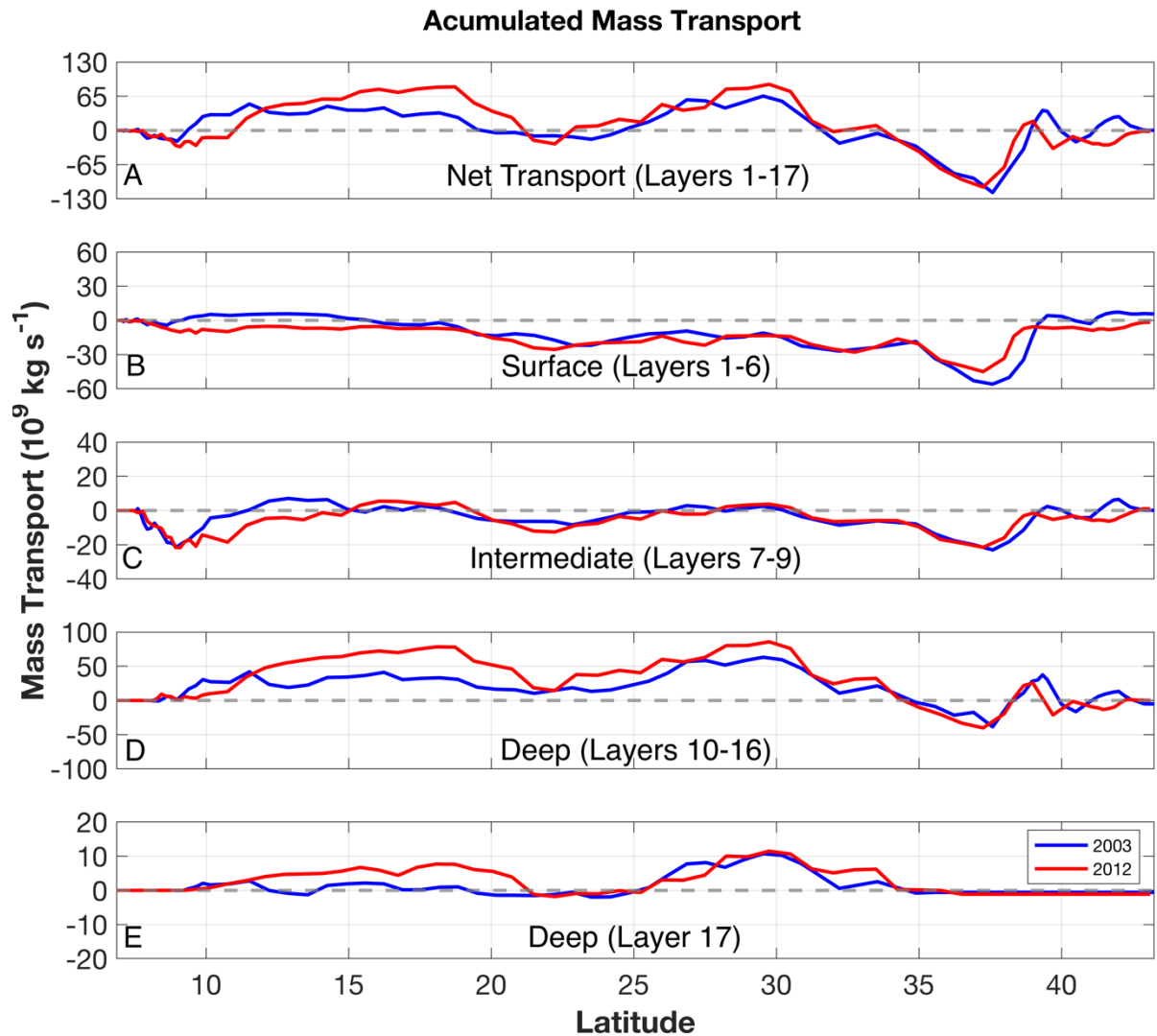


Figure 11. Northward accumulated mass transport (S_v) for the two cruises (blue lines for 2003 and red lines for 2012). A: Net transport (all layers). B: Surface transports (layers 1-6). C: Intermediate Transports (layers 7-9). D: Deep transports (layers 10-16). E: Bottom transport (layer 17).

5.1. Heat and Freshwater Transports

The heat and freshwater transports are estimated with the mass transports over the enclosed volume west of the A20 (Figs. 1, 10). Although mass conservation is imposed in each layer, water density conversions may be produced as a product of air-sea interactions (Hall et al. 2004), which may conclude with slight unbalances between layers. Fig. 10 shows a westward mass transport in the surface layers and an eastward transport at the intermediate-to-deep layers, thus as warmer and colder water masses flow on opposite directions heat fluxes may be carried with them. The net heat exchange is -0.52 ± 0.1 PW (1 PW = 10^{15} W) for 2003 and -0.58 ± 0.1 PW for 2012, yielding a slight increase in the overall heat absorbed by the ocean at 52°W for the studied decade. Our results are smaller than the results from Hall et al. (2004): -0.77 ± 0.1 PW.

The freshwater flux represents the unbalance between evaporation (negative) and precipitation and runoff (positive) that crosses the studied section. The oceanic-based freshwater fluxes are useful for the comparison with the meteorological ones as it is an independent way to estimate them. The freshwater flux has been computed as presented in Joyce et al. (2001) and resulted in 0.17 ± 0.08 Sv for 2003 and 0.13 ± 0.08 Sv for 2012, thus there is not a significant difference between both of them. The positive net values tell us that evaporation is weaker than precipitation+runoff over the basin enclosed by the A20 line. The same result but with a higher value was obtained by Hall et al. (2004): 0.55 ± 0.1 Sv, implying the possibility of seasonal-to-decadal variability.

6. Discussion

This study has estimated the transport of the main currents existing on the west North Atlantic Subtropical Gyre for 2003 and 2012, complementing the 1997 observation and allowing a deeper understanding of interannual variability. The meridionally integrated mass transport (Fig. 10A) shows slight changes between 2003 and 2012. Layer 4 ($26.0 < \sigma_t < 26.4$ kg m⁻³) presents a significant westward transport in 2003 that disappears in 2012, opposed to what occurred in layer 6 ($26.6 < \sigma_t < 27.0$ kg m⁻³): 2003 does not have a significantly different from zero transport but 2012 has a significant eastward transport. The first intermediate layer ($27.0 < \sigma_t < 27.5$ kg m⁻³) presents opposed transports for 2003 (westward) and 2012 (eastward). At the deep layer of $28.0 < \sigma_t < 28.05$ kg m⁻³, the 2012 transport is eastwards while in 2003 is not significantly different from zero. All these differences may be caused by seasonal and/or decadal changes, as it occurs with the GS and GSR (Pérez-Hernández & Joyce, 2014; Rayner et al., 2011; Tong Lee & Cornillon, 1995; Tracey & Watts, 1986). Moreover, the circulation pattern is not altered, but its magnitude changes as following: the LC decreases significantly between 2003 and 2012 while the NEC and the NBC increases (Table 2). The LC is weaker in this study than in 1997 because Hall et al. (2004) used a smaller range to estimate it (42.40-43.25°N) than us (39.25-43.1°N). Therefore, we may have just included some positive transports inside the LC's estimation as the Northern Recirculation Gyre may shift its position between years (Hogg et al., 1986). Compared to other studies, the decadal changes go even further beyond: it seems that the A20-crossing northern DWBC almost recovered the 1997 magnitude in 2012; the GS does not significantly change its magnitude between 2003-2012, but it surely does in comparison to 1997 (Table 2). The GSR is not altered between these 3 cruises and the southern DWBC seems to have increased its transport from 2003 onwards (Table 2).

The A22 is a section located at 66°W and occupied during the same years as the A20 used in this study. Relating the outcomes of this work to other sections where similar

inverse box models have been applied makes the observed changes more interesting: nor the northern and nor the southern DWBC shows significant changes between our estimations and the observations from 1997 described in Joyce et al. (2001), but the opposite occurred with the GS, which has considerably changed relative to 1997 at both 2003-2012 years (Table 2).

On one hand, the GS does not show any valuable differences between our 2003-2012 sections and the Casanova-Masjoan et al. (2018) 2003-2012 sections. On the other hand, the GSR was far more intense in both A20's 2003-2012 than in A22's 2003- 2012, as occurs also to our 2012's A20 southern DWBC and the 2012's Casanova-Masjoan et al. (2018) one. These differences may be caused by the range of latitudes used to estimate the transport, as the inverse model inputs are the same between our study and that of Casanova-Masjoan et al. (2018).

The intensification that appears between our 2012's northern and southern DWBC may be caused by a water mass entrainment along the DWBC paths from north to south, as described earlier by Casanova-Masjoan et al. (2018).

Table 2. Balanced transports (Sv) for the major current systems at the A20 described in this study and compared with previous results from Hall et al. (2004). For further comparison, the estimations of the A22 from Joyce et al. (2001) and Casanova-Masjoan et al. (2018) are also shown.

	A20 – 52°W			A22 – 66°W		
	This study		Hall et al. (2004)	Joyce et al. (2001)	Casanova-Masjoan et al. (2018)	
	2003	2012	1997	1997	2003	2012
North DWBC	-34.9±7.5	-25.3±9.4	-12.5	-37.5	-17.3±2.9	-14.9±2.5
LC	-0.80±1.4	-0.15±0.18	-8.6	-	-	-
GS	129.0±10.5	110.4±12.2	169	155.5	110.1±4.6	123.8±4.4
GSR	-88.2±12.0	-89.8±15.1	-80	-	-59.8±8.8	-43.0±10.9
NEC	-50.0±13.4	-91.7±12.0	-	-	-	-
NBC	-22.8±1.63	-32.0±1.80	-	-	-	-
South DWBC	42.0±8.0	48.0±8.1	32	44	30.9±10.3	17.6±8.6

Heat transports are larger for both years than the results from Casanova-Masjoan et al. (2018): -0.23 ± 0.08 PW (2003) and -0.21 ± 0.12 PW (2012). This may imply that the water volume enclosed by our section has larger differences between the southern warm inward transports and the northern cool outward transports than the water volume enclosed by A22 - 66°W.

Compared to Casanova-Masjoan et al. (2018) 2003-2012's negative-to-positive freshwater fluxes, ours did not show this seasonal change: it stayed positive for both years: 0.17 ± 0.08 Sv and 0.13 ± 0.08 Sv.

References

- Bower, A., Lozier, S., Biastoch, A., Drouin, K., Foukal, N., Furey, H., Lankhorst, M., Rühls, S., & Zou, S. (2019). Lagrangian Views of the Pathways of the Atlantic Meridional Overturning Circulation. In *Journal of Geophysical Research: Oceans* (Vol. 124, Issue 8, pp. 5313–5335). Blackwell Publishing Ltd. <https://doi.org/10.1029/2019JC015014>
- Casanova-Masjoan, M., Joyce, T. M., Pérez-Hernández, M. D., Vélez-Belchí, P., & Hernández-Guerra, A. (2018). Changes across 66°W, the Caribbean Sea and the Western boundaries of the North Atlantic Subtropical Gyre. *Progress in Oceanography*, 168, 296–309. <https://doi.org/10.1016/j.pocean.2018.09.013>
- Comas-Rodríguez, I., Hernández-Guerra, A., & Mcdonagh, E. L. (2010). Referencing geostrophic velocities using ADCP data at 24.5°N (North Atlantic). *Scientia Marina*, 74(2), 331–338. <https://doi.org/10.3989/scimar.2010.74n2331>
- Ganachaud, A. (2003). Large-scale mass transports, water mass formation, and diffusivities estimated from World Ocean Circulation Experiment (WOCE) hydrographic data. *Journal of Geophysical Research C: Oceans*, 108(7), 6–1. <https://doi.org/10.1029/2002jc001565>
- Hall, M. M., Joyce, T. M., Pickart, R. S., Smethie, W. M., & Torres, D. J. (2004). Zonal circulation across 52°W in the North Atlantic. *Journal of Geophysical Research: Oceans*, 109(11). <https://doi.org/10.1029/2003JC002103>
- Han, G., & Tang, C. L. (1999). Velocity and transport variability of the Labrador Current using TOPEX/Poseidon and hydrographic data. *Physics and Chemistry of the Earth, Part A: Solid Earth and Geodesy*, 24(4), 393–398. [https://doi.org/10.1016/S1464-1895\(99\)00047-2](https://doi.org/10.1016/S1464-1895(99)00047-2)
- Hernandez-Guerra, A., & Joyce, T. M. (2000). Water masses and circulation in the surface layers of the Caribbean at 66°W. *Geophysical Research Letters*, 27(21), 3497–3500. <https://doi.org/10.1029/1999GL011230>
- Hogg, N. G., Pickart, R. S., Hendry, R. M., & Smethie, W. J. (1986). The northern recirculation gyre of the gulf Stream. *Deep Sea Research Part A, Oceanographic Research Papers*, 33(9), 1139–1165. [https://doi.org/10.1016/0198-0149\(86\)90017-8](https://doi.org/10.1016/0198-0149(86)90017-8)
- Hormann, V., Lumpkin, R., & Foltz, G. R. (2012). Interannual North Equatorial Countercurrent variability and its relation to tropical Atlantic climate modes. *Journal of Geophysical Research: Oceans*, 117(C4), n/a-n/a. <https://doi.org/10.1029/2011JC007697>
- Joyce, T. M., Hernandez-Guerra, A., & Smethie, W. M. (2001). Zonal circulation in the NW Atlantic and Caribbean from a meridional World Ocean Circulation Experiment

- hydrographic section at 66°W. *Journal of Geophysical Research: Oceans*, 106(C10), 22095–22113. <https://doi.org/10.1029/2000JC000268>
- Joyce, T. M., Pickart, R. S., & Millard, R. C. (1999). Long-term hydrographic changes at 52 and 66°W in the North Atlantic Subtropical Gyre & Caribbean. *Deep Sea Research Part II: Topical Studies in Oceanography*, 46(1–2), 245–278. [https://doi.org/10.1016/S0967-0645\(98\)00102-7](https://doi.org/10.1016/S0967-0645(98)00102-7)
- Joyce, T. M., Thomas, L. N., Dewar, W. K., & Girton, J. B. (2013). Eighteen Degree Water formation within the Gulf Stream during CLIMODE. *Deep-Sea Research Part II: Topical Studies in Oceanography*, 91, 1–10. <https://doi.org/10.1016/j.dsr2.2013.02.019>
- Kanamitsu, M., Ebisuzaki, W., Woollen, J., Yang, S.-K., Hnilo, J. J., Fiorino, M., & Potter, G. L. (2002). NCEP–DOE AMIP-II Reanalysis (R-2). *Bulletin of the American Meteorological Society*, 83(11), 1631–1644. <https://doi.org/10.1175/BAMS-83-11-1631>
- Lillibridge, J. L., Hitchcock, G., Rossby, T., Lessard, E., Mork, M., & Golmen, L. (1990). Entrainment and mixing of shelf/slope waters in the near-surface Gulf Stream. *Journal of Geophysical Research*, 95(C8), 13065. <https://doi.org/10.1029/jc095ic08p13065>
- Little, C. M., Hu, A., Hughes, C. W., McCarthy, G. D., Piecuch, C. G., Ponte, R. M., & Thomas, M. D. (2019). The Relationship Between U.S. East Coast Sea Level and the Atlantic Meridional Overturning Circulation: A Review. In *Journal of Geophysical Research: Oceans* (Vol. 124, Issue 9, pp. 6435–6458). Blackwell Publishing Ltd. <https://doi.org/10.1029/2019JC015152>
- Macdonald, A. M. (1998). The global ocean circulation: A hydrographic estimate and regional analysis. *Progress in Oceanography*, 41(3), 281–382. [https://doi.org/10.1016/S0079-6611\(98\)00020-2](https://doi.org/10.1016/S0079-6611(98)00020-2)
- Metcalf, W. G. (1976). Caribbean-Atlantic water exchange through the Anegada-Jungfern passage. *Journal of Geophysical Research*, 81(36), 6401–6409. <https://doi.org/10.1029/JC081i036p06401>
- Pérez-Hernández, M. D., Hernández-Guerra, A., Fraile-Nuez, E., Comas-Rodríguez, I., Benítez-Barrios, V. M., Domínguez-Yanes, J. F., Vélez-Belchí, P., & De Armas, D. (2013). The source of the Canary current in fall 2009. *Journal of Geophysical Research: Oceans*, 118(6), 2874–2891. <https://doi.org/10.1002/jgrc.20227>
- Pérez-Hernández, M. D., & Joyce, T. M. (2014). Two modes of Gulf Stream variability revealed in the last two decades of satellite altimeter data. *Journal of Physical Oceanography*, 44(1), 149–163. <https://doi.org/10.1175/JPO-D-13-0136.1>
- Pérez-Hernández, M. D., McCarthy, G. D., Vélez-Belchí, P., Smeed, D. A., Fraile-Nuez, E., & Hernández-Guerra, A. (2015). The Canary basin contribution to the seasonal cycle of the Atlantic meridional overturning circulation at 26°N. *Journal of Geophysical Research: Oceans*, 120(11), 7237–7252. <https://doi.org/10.1002/2015JC010969>
- Pérez-Hernández, M. Dolores, Pickart, R. S., Torres, D. J., Bahr, F., Sundfjord, A., Ingvaldsen, R., Renner, A. H. H., Beszczynska-Möller, A., Appen, W., & Pavlov,

- V. (2019). Structure, Transport, and Seasonality of the Atlantic Water Boundary Current North of Svalbard: Results From a Yearlong Mooring Array. *Journal of Geophysical Research: Oceans*, 124(3), 1679–1698. <https://doi.org/10.1029/2018JC014759>
- Rayner, D., Hirschi, J. J. M., Kanzow, T., Johns, W. E., Wright, P. G., Frajka-Williams, E., Bryden, H. L., Meinen, C. S., Baringer, M. O., Marotzke, J., Beal, L. M., & Cunningham, S. A. (2011). Monitoring the Atlantic meridional overturning circulation. *Deep-Sea Research Part II: Topical Studies in Oceanography*, 58(17–18), 1744–1753. <https://doi.org/10.1016/j.dsr2.2010.10.056>
- Sato, O. T., & Rossby, T. (1995). Seasonal and low frequency variations in dynamic height anomaly and transport of the Gulf Stream. *Deep-Sea Research Part I*, 42(1), 149–164. [https://doi.org/10.1016/0967-0637\(94\)00034-P](https://doi.org/10.1016/0967-0637(94)00034-P)
- Smethie, W. M. (1993). Tracing the thermohaline circulation in the western North Atlantic using chlorofluorocarbons. In *Progress in Oceanography* (Vol. 31, Issue 1, pp. 51–99). Pergamon. [https://doi.org/10.1016/0079-6611\(93\)90023-7](https://doi.org/10.1016/0079-6611(93)90023-7)
- Talley, L. D., Feely, R. A., Sloyan, B. M., Wanninkhof, R., Baringer, M. O., Bullister, J. L., Carlson, C. A., Doney, S. C., Fine, R. A., Firing, E., Gruber, N., Hansell, D. A., Ishii, M., Johnson, G. C., Katsumata, K., Key, R. M., Kramp, M., Langdon, C., Macdonald, A. M., ... Zhang, J.-Z. (2016). Changes in Ocean Heat, Carbon Content, and Ventilation: A Review of the First Decade of GO-SHIP Global Repeat Hydrography. *Annual Review of Marine Science*, 8(1), 185–215. <https://doi.org/10.1146/annurev-marine-052915-100829>
- Tong Lee, & Cornillon, P. (1995). Temporal variation of meandering intensity and domain-wide lateral oscillations of the Gulf Stream. *Journal of Geophysical Research*, 100(C7), 13603–13613. <https://doi.org/10.1029/95jc01219>
- Tracey, K. L., & Watts, D. R. (1986). On Gulf Stream meander characteristics near Cape Hatteras. *Journal of Geophysical Research*, 91(C6), 7587. <https://doi.org/10.1029/jc091ic06p07587>
- Våge, K., Pickart, R. S., Spall, M. A., Moore, G. W. K., Valdimarsson, H., Torres, D. J., Erofeeva, S. Y., & Nilsen, J. E. Ø. (2013). Revised circulation scheme north of the Denmark Strait. *Deep-Sea Research Part I: Oceanographic Research Papers*, 79, 20–39. <https://doi.org/10.1016/j.dsr.2013.05.007>
- Vélez-Belchí, P., Pérez-Hernández, M. D., Casanova-Masjoan, M., Cana, L., & Hernández-Guerra, A. (2017). On the seasonal variability of the Canary Current and the Atlantic Meridional Overturning Circulation. *Journal of Geophysical Research: Oceans*, 122(6), 4518–4538. <https://doi.org/10.1002/2017JC012774>
- Wunsch, C. (1978). The North Atlantic general circulation west of 50°W determined by inverse methods. In *Reviews of Geophysics* (Vol. 16, Issue 4, pp. 583–620). John Wiley & Sons, Ltd. <https://doi.org/10.1029/RG016i004p00583>
- Wunsch, C. (1996). The Ocean Circulation Inverse Problem. In *The Ocean Circulation Inverse Problem*. Cambridge University Press. <https://doi.org/10.1017/cbo9780511629570.006>